이학석사 학위논문

Structural analysis of carbon monoxide dehydrogenase (CODH) with enhanced oxygen resistance

산소저항성을 높인

carbon monoxide dehydrogenase (CODH)의

구조 규명 연구

2024 년 2 월

서울대학교 대학원

화학부 생화학 전공

공 소 연

Structural analysis of carbon monoxide dehydrogenase (CODH) with enhanced oxygen resistance

지도 교수 이 형 호

이 논문을 이학석사 학위논문으로 제출함

2023 년 12 월

서울대학교 대학원

화학부 생화학 전공

공 소 연

공소연의 이학석사 학위논문을 인준함

2024 년 1 월

위 원 장 _____ 김 석 희 _____ (인)

부위원장 _____ 이 형 호 _____ (인)

위 원 _____ 송 윤 주 _____ (인)

Abstract

Carbon monoxide dehydrogenase *(Ch*CODH-II*)* from *Carboxydothermus hydrogeno formans* is an anaerobic bacteria catalyzing the oxidation of CO to CO_2. While this enzyme has the highest conversion rate compared to other CODHs, it is sensitive to oxygen, limiting practical applications. To overcome this limitation, the previous study focused on introducing mutations involving histidine, tryptophan, and serine residues with bulky aromatic rings at the internal bottleneck site of the gas tunnel connected to the C-cluster, as residue A559. However, these variants maintained activity only under low oxygen concentrations (0.1-0.5% O_2). Therefore, in this study, *Ch*CODH-II variants were developed that retain CO version activity even under atmospheric oxygen conditions (20% O_2). Additional mutations were introduced at V610 to histidine or tryptophan, which are in close proximity to the non-selective tunnel while being connected to the C-cluster. Through X-ray crystallography of the variants under anaerobic conditions, I demonstrated the reason for the enhanced oxygen resistance. Furthermore, tunnel analysis revealed that introduced mutations resulted in the narrowing of the tunnel entrances around the mutated residues when compared to the *Ch*CODH-II WT. To investigate the structural integrity of the mutants under oxygen exposure, anaerobically purified proteins were exposed to 2 hours of oxygen, and then crystallization was conducted under anaerobic conditions. Omit maps (*Fo-Fc*) and Fe

anomalous maps showed that C and D clusters of *Ch*CODH-II WT were damaged, while the WH (A559W/V610H) variant retained its structural integrity. Tunnel analysis further confirmed that the tunnels had narrowed, consistent with the results obtained from crystallization under anaerobic conditions. It was shown that introducing mutations involving histidine and tryptophan, which have large aromatic rings, into A559 and V610 results in the constriction of non-selective gas tunnels, dramatically blocking O_2 gas and enhancing O_2 resistance.

Keywords : Carbon monoxide dehydrogenase, *Ch*CODH-II, protein structure, O_2 tolerance, CO reduction

Student number : 2021-27351

Table of Contents

Figure Contents

Table Contents

1. Introduction

1.1. Study Background

A large amount of carbon monoxide (CO) is generated from both natural sources and human activities (Ragsdle et al., 2004). According to the OECD database (https://stats.oecd.org, air emissions source in 2017), carbon monoxide (CO) constitutes a more significant proportion of atmospheric pollutants than carbon dioxide (CO_2), so many efforts are needed to reduce its emissions. CO gas has energetically rich chemical bonds, so it can be transformed into environmentally friendly energy sources and chemicals (Kim et al., 2022). To efficiently convert CO into a cost-effective and recyclable energy source, utilizing highly substrate-selective carbon monoxide dehydrogenase (CODH) enzymes found in bacteria and archaea is crucial, as these enzymes can facilitate the conversion of CO into CO_2 (Kim et al., 2016). CODH enzymes can be classified into two families based on the metal composition and distribution at the active site (Choi et al., 2017; Domnik et al., 2017; Jeoung et al., 2019), resulting in [(CuSMo(O)O) and ($CuSMo(O)OH_2$)] cluster (Rovaletti et al., 2019) for Mo- and Cu- containing CODH (E.C.1.2.5.3) and [$NiFe_3$ S_4OH_X] clusters for Ni-Fe CODHs (Dobbek et al., 2001; Dobbek et al., 2004; Drennan et al., 2001). These CODH enzymes exhibit a moderate rate of CO conversion (93.3 s^{-1}) under aerobic

conditions (Zhang et al., 2010), but under anaerobic conditions, a significantly higher rate of CO conversion (31,000 s^{-1}) occurs. Remarkably, *Carboxydothermus hydrogenoformans* (*Ch*CODH-IV) (Domnik et al., 2017) and *Desulfovibrio vulgaris* (*Dv*CODH) (Merrouch et al., 2015), unlike other CODHs, are less oxygen sensitive. To effectively apply CODHs in industrial fields, it was necessary to enhance the oxygen tolerance of *Ch*CODH-II, which has the highest CO oxidation rate but is O_2 sensitive (Kim et al., 2022). By comparing its protein sequence and structure with the O_2-resistant *Ch*CODH-IV, mutations were introduced at the A559 site with tryptophan, histidine, and serine amino acid, and these mutations resulted in a remarkable O_2 tolerance compared to the wild type (Kim et al., 2022).

However, the single variants (A559W, A559H, A559S) have a limitation in that the CO conversion rate is only within the range of industrial waste gas conditions (0.1-0.5% O_2). To maintain activity even under atmospheric conditions (20% O_2), the bottleneck near the surface located at the V610 site was identified in the non-selective tunnel based on *Ch*CODH-II (WT & A559W). To further enhance the O_2 resistance, I obtained the crystal structures of the variants and analyzed the local environmental change in the A559 and V610 residues. Also, tunnel analysis confirmed that these mutations selectively block only H_2O or O_2 without affecting the main CO tunnel, resulting in a reduction in the gas tunnel surrounding the mutation sites compared to *Ch*CODH-II WT (PDB ID:1SU7). Finally, we demonstrated a

more powerful potential for industrial utilization by employing engineered CODHs with high CO oxidation rates, even under 20% O_2 conditions, for CO removal. It suggests the feasibility of developing and promoting environmentally friendly and effective CO removal and gas purification processes in the industrial field.

1.2. Discovery of the mutants to increase the O_2 tolerance[1]

To enhance the oxygen resistance of Ni-Fe-CODHs, a comparative analysis of the protein sequences and tunnel analysis was conducted on O_2-sensitive *Ch*CODH-II and less O_2-sensitive *Ch*CODH-IV, *Dv*CODH, and *Rr*CODH (Figure 1.1A). In the previous study, both *Ch*CODH-IV and *Dv*CODH were identified to have five residues (D94, E101, R187, Y558, and Q559) that differed from *Ch*CODH-II (Kim et al., 2022). Among these residues, it was hypothesized that the Y558 residue, positioned near the tunnel, showed an important role in the oxygen resistance of *Ch*CODH-IV. They mutated A559 to more significant aromatic residues, such as tryptophan, histidine, and serine to mimic this role. However, a limitation was observed as mutating only the internal bottleneck, A559, provided oxygen resistance under low oxygen conditions (typically 0.1-0.5% O_2). Additional bottleneck sites for

[1] The mutants to increase the O_2 tolerance were discovered by Suk Min Kim, Ph. D. in Ulsan National Institute of Science and Technology (UNIST).

mutation were introduced to get higher oxygen resistance. Through tunnel analysis, three branches were identified near the surface in a tunnel that was believed to be a non-selective CO tunnel (water tunnel) connected to the active site C-cluster. These bottleneck sites in the tunnel were designated as nonselective tunnel 1 (E43, K450, L583), tunnel 2 (I586, T593, V610), and tunnel 3 (Q206, S599, I603) (Figure 1.1B). Mutation studies were conducted on these sites, and based on the results, V610 was selected as the most promising mutation residue due to its ability to enhance O_2 tolerance while maintaining the highest expression level (Appendix).

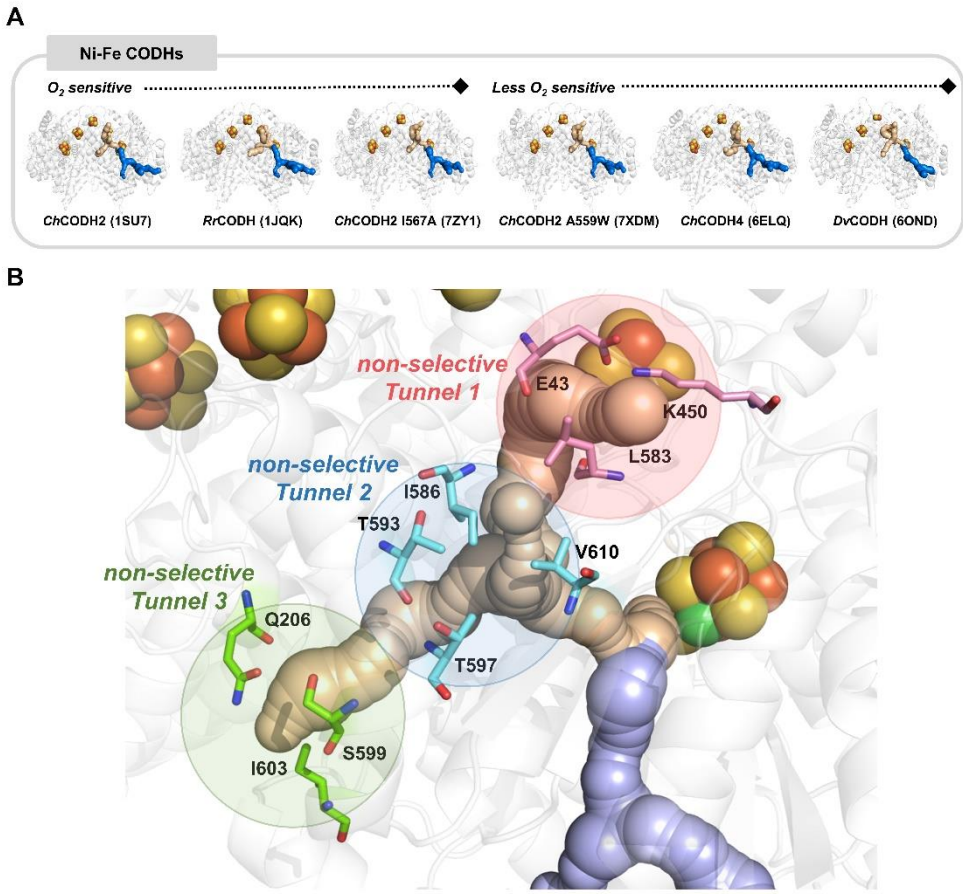

Figure 1.1 Discovery of key residue for O_2 tolerance in ChCODH-II from tunnel analysis and sequence alignment

A. Tunnel analysis of Ni-Fe CODHs; A comparison of tunnels between the less oxygen-sensitive A559W mutation and *Ch*CODH-IV and *Dv*CODH, and the oxygen-sensitive *Ch*CODH-II and *Rr*CODH. **B.** Surface bottleneck point of non-selective gas tunnels connected to the active site of C-clusters. The non-selective tunnel divides into three branches on the surface.

2. Material and Methods

2.1. Expression[2] and purification of *Ch*CODH-II mutants and WT

The expression of CODH constructs was carried out as described previously (Kim et al., 2022). Briefly, cultures were grown in a modified TB medium at 37℃. When the culture reached an OD600 of 0.4-0.6, 0.2 mM IPTG with $NiCl_2$, $FeSO_4$, and KNO_3 at 30℃ after N_2-fluxing was induced. After overnight induction at 30℃, the cells were harvested and stored aerobically at –70℃. All the purification steps were conducted in an anoxic glove box (model B, COY Laboratory Products Inc., Michigan, USA) under an atmosphere of N_2/ H_2(v/v) at room temperature. Sonication was carried out anaerobically on ice. Cell lysates were centrifuged and purified by Ni-NTA affinity chromatography (Qiagen) and size exclusion chromatography (HiLoad 16/600 Superdex 200 prep grade, GE Healthcare Bio-Science, PA, USA) in an anoxic glove box (model B, COY Laboratory Products Inc., Michigan, USA), as described previously (Kim et al., 2022). For the crystallization, the final buffer condition of the protein was 20 mM Tris-HCl pH7.5 and 3 mM DTE, and all samples were stored at 4℃. When the purified protein was running with SDS PAGE (Sodium dodecyl sulfate-

[2] Expression of *Ch*CODH-II mutants was performed by Jinhee Lee in Ulsan National Institute of Science and Technology (UNIST).

polyacrylamide gel electrophoresis on 10% gels), the His6-tag and the calculated protein size merged, confirming a size of 69 kDa, and the protein concentration was measured using the Bradford method (Figure 2.2). Regarding the time oxygen exposure experiment of *Ch*CODH-II A559W/V610 variant and WT was performed in the anoxic glove box, the protocol was the same as under anaerobic conditions. The purified anaerobic protein was taken outside the glove box and exposed to oxygen for 2 hours before the anaerobic crystallization (Figure 2.1C).

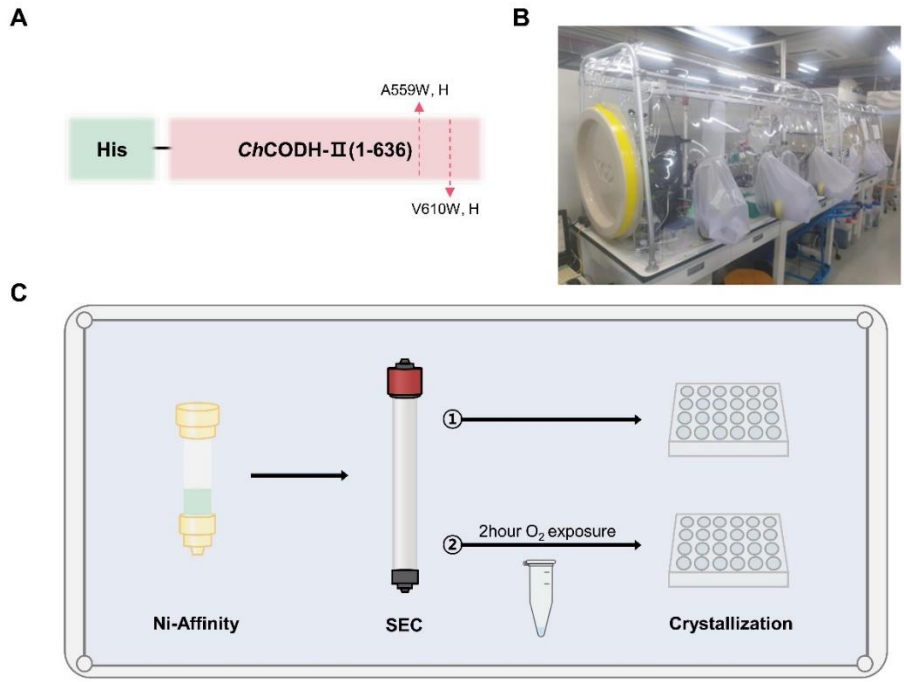

Figure 2.1 Construct design and purification and crystallization process of *Ch*CODH-II A559 / V610 variants and WT.

A. Construct of *Ch*CODH-II A559 variants. **B.** Anaerobic chamber for protein purification and crystallization. **C.** Process of anaerobic crystallization experiment and 2 h oxygen exposure experiment

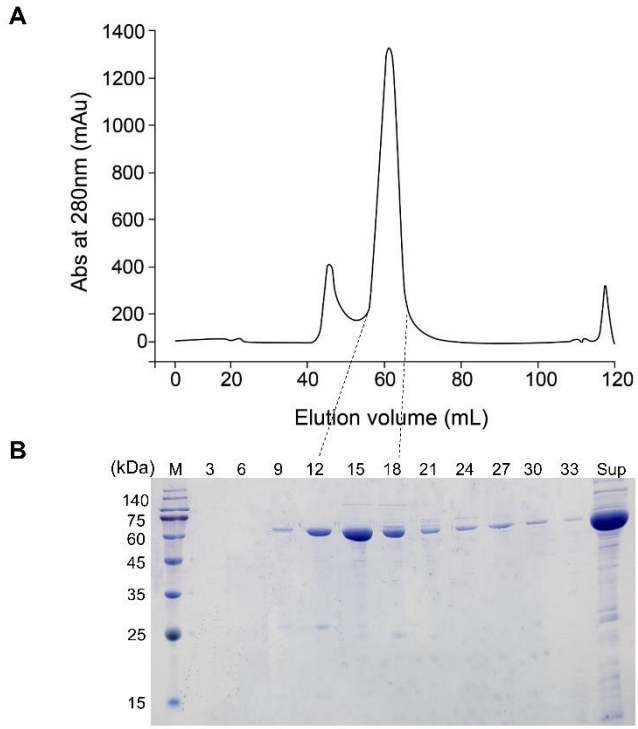

Figure 2.2 Purification of *Ch*CODH-II A559/V610 variants

A. UV peak of size-exclusion chromatography (HiLoad 16/600 Superdex 200 prep grade, GE Healthcare) and SDS-PAGE gel for *Ch*CODH-II A559W/V610H variant. Other mutants were same as above.

2.2. Crystallization of *Ch*CODH-II mutants and WT

To make anaerobic crystals of *Ch*CODH-II WH (A559W/V610H), WW (A559W/V610W), and HH (A559H/V610H) variants, crystals were grown anaerobically at 22°C using the hanging drop method. They were combining the 2 µl of protein (10 mg/ml) with 2 µl of reservoir solution consisting of 0.1 M HEPES/NaOH pH 7.0, 0.2 M $MgCl_2$, and 25% (w/v) polyethylene glycol 3,350 on a glass cover slide and sealed over a reservoir containing 500 µl solution. Crystals were transferred in a cryoprotectant solution containing the reservoir solution with 10% (w/v) glycerol.

To obtain the crystal with time-exposed oxygen, the anaerobically purified protein was exposed to oxygen for 2 hours before undergoing anaerobically crystallization. The crystallization method was performed using the same procedure as described above.

2.3. Crystallographic data collection and structure determination

All data were collected at the Pohang Light Source (PLS) on 5C Beamlines, and the SPring8 (SP8) beamlines at a temperature of 100 K. Native data were collected at a wavelength of 0.8999 and 1.0000 Å and Fe peak data at 1.736 Å. The crystals were diffracted to resolutions of 2.1 Å, 2.0 Å, 1.83 Å, 2.7 Å, and 2.0 Å. All data were integrated and scaled using the HKL2000 software package (Otwinowski and Minor, 1997a) and XDS (Kabsch, 2010). Data collection statistics are summarized in Table 2.1-2.2. Structures were solved by molecular replacement (MR) using the previously published *Ch*CODH-II WT (PDB ID:1SU7) and single mutant A559W (PDB ID:7XDM). Model building was performed using the CCP4 Molrep (Winn et al., 2011). Following MR, Subsequent manual model building was performed using the Coot (Emsley and Cowtan, 2004), and refinement was carried out in Phenix (Liebschner et al., 2019) and CCP4 refmac5 in the absence of hydrogen atoms. Several rounds of model building, including positional refinement, Ramachandran statistics, atomic coordinates, and B-factor, refinement were performed in Coot and Phenix. Water molecules were automatically added in Phenix and fitting by either removing or adding using Coot to match the stable number of water molecules. The final refinement models were validated using omit map and Fe anomalous map calculated in Phenix. All refinement statistics are summarized in Table. Figures were generated in PyMOL.

Table 2.1 Data collection and refinement statistics for structures of anaerobic A559/V610 variants

	Anaerobic A559W/V610H	Anaerobic A559W/V610W	Anaerobic A559H/V610H
Data collection			
Space group	*C*2	*C*2	*C*2
Wavelength (Å)	1.0000	1.0000	1.0000
Cell dimensions			
a, *b*, *c* (Å)	112.2, 75.8, 71.4	112.0, 75.5, 71.5	111.9, 75.3, 70.9
α, β, γ (°)	90, 111.5, 90	90, 111.8, 90	90, 111.2, 90
Resolution (Å)	50-2.1 (2.10-2.14)[a]	50-2.0 (2.00-2.03)[a]	50-2.1 (2.14-2.10)[a]
Total / Unique reflections	217,452/32,319	250,025/37,021	315,858/47,694
R_{merge}[b] (%)	8.7 (40.7)[a]	8.3 (69.2)[a]	8.8 (71.9) [a]
$CC_{1/2}$	99.4 (92.9)[a]	99.2 (84.1)[a]	99.5 (81.8)[a]
$I/\sigma I$	19.3 (3.5)[a]	20.3 (2.5)[a]	20.1 (1.7)[a]
Completeness (%)	99.0 (98.3)[a]	99.0 (100)[a]	98.7 (90.4)[a]
Redundancy	6.7 (6.6)[a]	6.8 (6.7)[a]	6.6 (5.3)[a]
Model refinement statistics			
Resolution range (Å)	50-2.10	50-2.00	50-2.10
R_{work} / R_{free}[c] (%)	16.4 / 21.1	17.0/ 21.8	17.0/ 21.8
No. atoms			
Protein	4,665	4,683	4,618
Cluster	22	22	22
water	250	254	337
Average *B*-factor (Å^2)			
Protein	27.3	28.2	22.0
Cluster	29.6	29.5	30.6
Water	30.0	30.5	27.2

RMSDs from ideal geometry			
Bond lengths (Å)	0.008	0.008	0.008
Bond angles (°)	0.967	0.967	0.935
Protein-geometry analysis (%)			
Ramachandran preferred	94.8	94.9	94.3
Ramachandran allowed	4.6	4.5	5.2
Ramachandran outliers	0.6	0.6	0.5

[a]Values in parentheses refer to the highest resolution shell.

[b]$R_{merge} = \Sigma_{hkl}\Sigma_i \mid I_i(hkl) - \langle I(hkl)\rangle \mid / \Sigma_{hkl}\Sigma_i I_i(hkl)_i$, where $I(hkl)$ is the intensity of reflection hkl, Σ_{hkl} is the sum over all reflections, and Σ_i is the sum over i measurements of reflection hkl.

[c]$R = \Sigma hkl||Fobs|-|Fcalc|\ |/\Sigma hkl|Fobs|$, where R_{free} was calculated for a randomly chosen 5% of reflections, which were not used for structure refinement, and R_{work} was calculated for the remaining reflections.

Table 2.2 Data collection and refinement statistics for structures of 2 h oxygen exposure WH (A559W/V610) & WT

	O_2-exposed 2h A559W/V610H	O_2-exposed 2h WT
Data collection		
Space group	*C*2	*C*2
Wavelength (Å)	1.0000	0.9000
Cell dimensions		
a, *b*, *c* (Å)	112.6, 75.9, 71.8	111.3, 75.6, 70.7
α, β, γ (°)	90.0, 112.1, 90.0	90.0, 110.0, 90.0
Resolution (Å)	50-2.0	50-2.7
Total / Unique reflections	230,027/38,012	104,510/15,150
R_{merge}[b] (%)	3.8 (19.4)[a]	6.3 (73.6)[a]
$CC_{1/2}$	99.9 (98.0)[a]	99.9 (84.4)[a]
$I/\sigma I$	29.7 (7.9)[a]	14.8 (2.2)[a]
Completeness (%)	99.7 (99.4)[a]	99.4 (98.6)[a]
Redundancy	6.1 (6.2)[a]	6.9 (7.1)[a]
Model refinement statistics		
Resolution range (Å)	50-2.00	50-2.70
R_{work} / R_{free}[c] (%)	18.3 / 22.7	19.3/ 27.4
No. atoms		
Protein	4,622	4,610
Cluster	22	22
water	206	-
Average *B*-factor (Å^2)		
Protein	28.5	95.4
Cluster	45.1	147.5
Water	30.9	-
RMSDs from ideal geometry		
Bond lengths (Å)	0.009	0.015

Bond angles (°)	1.012	1.579
Protein-geometry analysis (%)		
Ramachandran preferred	95.3	90.7
Ramachandran allowed	4.1	7.9
Ramachandran outliers	0.6	1.4

[a]Values in parentheses refer to the highest resolution shell.

[b]$R_{merge} = \Sigma_{hkl}\Sigma_i \mid I_i(hkl) - \langle I(hkl)\rangle \mid / \Sigma_{hkl}\Sigma_i I_i(hkl)_i$, where $I(hkl)$ is the intensity of reflection hkl, Σ_{hkl} is the sum over all reflections, and Σ_i is the sum over i measurements of reflection hkl.

[c]$R = \Sigma hkl||Fobs|-|Fcalc| |/\Sigma hkl|Fobs|$, where R_{free} was calculated for a randomly chosen 5% of reflections, which were not used for structure refinement, and R_{work} was calculated for the remaining reflections

2.4. Fe anomalous difference map

The anomalous diffraction data were collected at the peak position of the iron absorption edge (1.7364 Å). Anomalous data were processed and scaled using the HKL2000 software package and XDS. An anomalous difference Fourier map calculation was carried out using the Phenix. Data collection statistics are summarized in Table 2.3-2.4.

Table 2.3 Statistics for anomalous data collection and refinement

	Anaerobic A559W/V610H	Anaerobic A559W/V610W	Anaerobic A559H/V610H
Data collection			
Space group	*C*2	*C*2	*C*2
Cell dimension			
a, *b*, *c* (Å)	112.1, 76.1, 71.8	112.3, 76.0, 72.1	112.3, 75.7, 71.5
α, β, γ (°)	90.0, 112.1, 90.0	90.0, 112.2. 90.0	90.0, 111.4, 90.0
wavelength (Å)	1.7364	1.7364	1.7364
Resolution (Å)	50–2.85	50-2.89	50-2.20
R_{merge}[b] (%)	4.0 (6.8) [a]	4.3 (7.5) [a]	5.1 (25.5) [a]
$CC_{1/2}$	99.6 (99.0) [a]	99.6 (99.0) [a]	99.7 (94.8) [a]
Completeness (%)	94.6 (94.7) [a]	92.6 (93.0) [a]	98.9 (96.0) [a]
Redundancy	2.3 (2.3) [a]	2.4 (2.4) [a]	3.5 (3.4) [a]

[a]Values in parentheses refer to the highest resolution shell.

[b]$R_{merge} = \Sigma_{hkl}\Sigma_i \mid I_i(hkl) - \langle I(hkl)\rangle \mid / \Sigma_{hkl}\Sigma_i I_i(hkl)_i$, where $I(hkl)$ is the intensity of reflection *hkl*, Σ_{hkl} is the sum over all reflections, and Σ_i is the sum over i measurements of reflection *hkl*.

Table 2.4 Statistics for anomalous data collection and refinement of oxygen exposure

	O_2-exposed 2 h A559W/V610H	**O_2-exposed 2 h WT**
Data collection		
Space group	*C*2	*C*2
Cell dimension		
a, *b*, *c* (Å)	112.4, 76.3, 71.8	111.8, 76.1, 70.9
α, β, γ (°)	90.0, 111.7, 90.0	90.0, 111.2, 90.0
wavelength (Å)	1.7364	1.7364
Resolution (Å)	50-1.8	50-2.6
R_{merge}[b] (%)	4.8 (26.9)[a]	6.2 (70.9)[a]
$CC_{1/2}$	99.8 (92.5)[a]	99.9 (75.9)[a]
Completeness (%)	98.3 (94.6)[a]	99.4 (98.6)[a]
Redundancy	3.3 (3.2)[a]	3.5 (3.5)[a]

[a]Values in parentheses refer to the highest resolution shell.

[b]$R_{merge} = \Sigma_{hkl}\Sigma_i \mid I_i(hkl) - \langle I(hkl)\rangle \mid / \Sigma_{hkl}\Sigma_i I_i(hkl)_i$, where $I(hkl)$ is the intensity of reflection *hkl*, Σ_{hkl} is the sum over all reflections, and Σ_i is the sum over i measurements of reflection *hkl*.

3. Results

3.1. Crystal structures and local changes in A559/ V610 mutation site

To find the reasons for further enhanced oxygen resistance in *Ch*CODH-II A559/V610 mutants, I solved the crystal structures of the variants A559W/V610, A559W/V610W, and A559H/V610H under anaerobic condition. In a previous study (Kim et al., 2022), the A559 site, located at the internal bottleneck of the non-selective tunnel mutated to tryptophan, histidine, and serine. However, activity was observed only under low oxygen (0.1-0.5% O_2) conditions. To overcome the limitation, an additional mutation at V610 was introduced to maintain CO oxidation activity even under high oxygen (20% O_2) conditions. The hanging drop method was conducted in the anaerobic chamber to make anaerobic crystals. Large and yellow crystals were successfully obtained, leading to high-resolution data collection. Firstly, I examined the local changes surrounding the A559 mutation residues by comparing them to *Ch*CODH-II WT (PDB ID: 1SU7) (Figure 3.1B). In the case of the A559W or A559H double mutants, the results were consistent with previous findings. The side chain of I580 was pushed away through the introduction of the bulkier residue W559 or H559 instead of alanine. Additionally, interactions with Asn448 and a new hydrogen bond with Val582 were observed. Secondly, the local changes resulting from the V610 mutation were observed (Figure 3.1B). The V610 site is located at the surface

bottleneck of the non-selective tunnel 2. In the case of the 610 residue, where valine was mutated to the larger aromatic residue histidine, it was demonstrated that the mutation sites did not interrupt the neighboring residues, thus effectively preserving structural integrity. The bulky aromatic ring also effectively obstructed oxygen entrance near the protein surface, contributing to increased oxygen tolerance. Conversely, in the case of the V610W mutant, introducing tryptophan with a larger aromatic ring led to increased flexibility, resulting in a disordered state. The two locations could be broadly categorized: V610H-like mutations did not significantly affect I580, L583, or L612, while mutations at other positions impacted the preceding three residues (Figure 3.2C).

In summary, the incorporation of mutations at A559 and V610 not only blocked internal oxygen entrance but also hindered oxygen ingress near the surface. As a result, the double mutants effectively increased oxygen resistance.

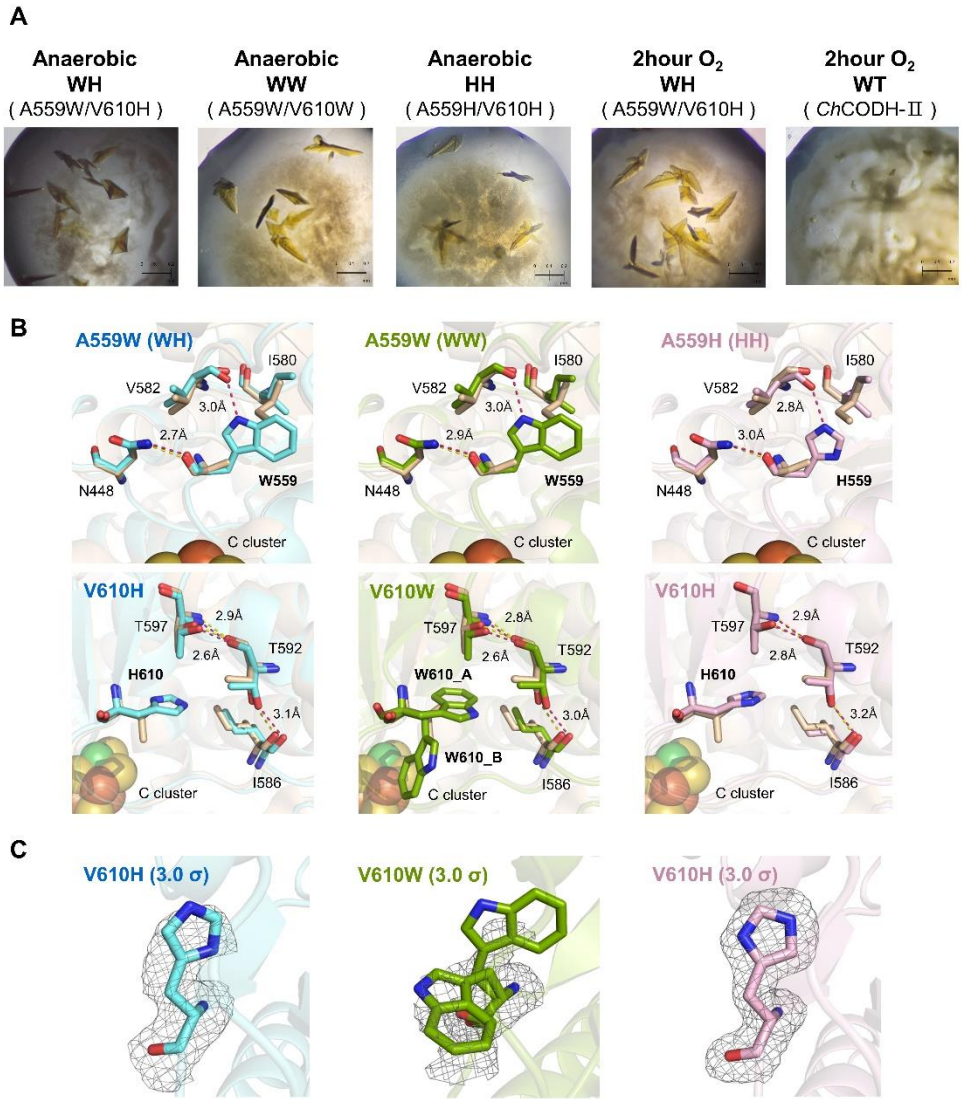

Figure 3.1 Crystal structures of *Ch*CODH-II A559/V610 variants and local environments in A559/V610 sites

A. A559/V610 double variants crystal pictures of Anaerobic and 2 h oxygen exposure conditions (microscope magnified 5X) **B.** Local environments around A559 mutations sites. **C.** Omit map (*Fo-Fc*) of V610 site in anaerobic A559/V610 variants.

3.2. Electron density map and Fe anomalous map in clusters

*Ch*CODH-II has three iron-sulfur clusters known as B, C, and D clusters and it exists as a dimer to facilitate electron transfer generated from CO oxidation. Previous studies had identified the D cluster as a [2Fe-2S], the B cluster [4Fe-4S], and the C cluster as either a [Ni-4Fe-4S] or [Ni-4Fe-5S] configuration. Specifically, the C-cluster is the active site for CO and CO_2 conversion, with electrons generated during these reactions and transferring to the B and D clusters. To certify the integrity of the clusters in the variants despite the mutations, I compared the omit map (Figure 3.2) and Fe anomalous map (Figure 3.3) to the *Ch*CODH- II WT (PDB ID:1SU7). The positions and interacting residues around the D, B, and C clusters in the variants closely resembled *Ch*CODH-II WT with minimal deviation values. In anaerobic A559W/V610H, A559W/V610W and A559H/V610H variants, the RMSD values for each cluster compared to the *Ch*CODH- II WT are as follows (B clusters: 0.025 Å, 0.029 Å and 0.032 Å for 8 atoms: C clusters: 0.272 Å, 0.270 Å and 0.353 Å for 10 atoms; D clusters: 0.049 Å, 0.052 Å, and 0.048 Å for 4 atoms). This observation confirms the presence of Fe in all clusters and the overall structural integrity of the clusters. Unexpectedly, the A559W/V610W variant preserved the cluster integrity; however, the W610 site was disordered due to incorporating an excessively bulky aromatic residue. Analyzing the four variants, the HH (A559H/V610H) variant exhibited slightly higher oxygen resistance but lower protein stability. The WW (A559W/V610W)

variant was disordered at 610 site. The inability of the HW (A559H/V610W) variant to crystallize can be attributed to reasons identified in the HH and WW mutants. Therefore, I concluded that the WH (A559W/V610H), which has higher protein stability, ordered mutation residues, and oxygen resistance, is the most appropriate model among the variants.

	D cluster (3.0 σ)	B cluster (3.0 σ)	C cluster (3.0 σ)
ChCODH2 WT PDB : 1SU7	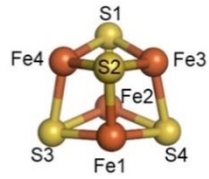	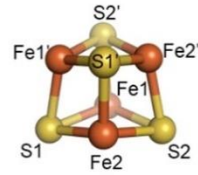	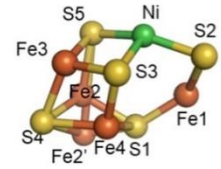
Anaerobic WH (A559W/V610H)	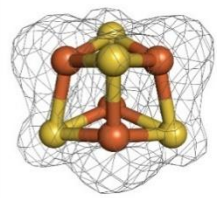	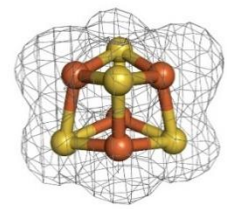	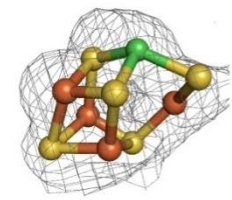
Anaerobic WW (A559W/V610W)	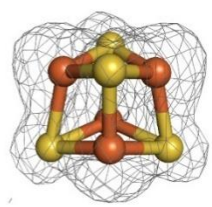	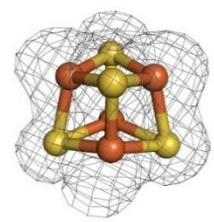	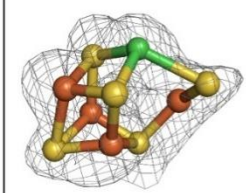
Anaerobic HH (A559H/V610H)	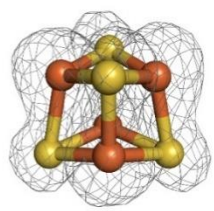	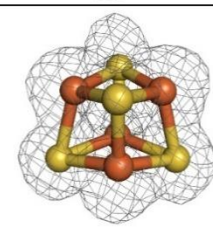	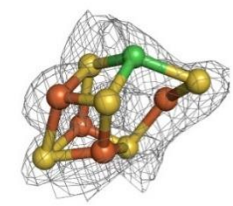

Figure 3.2 $F_o - F_c$ difference electron density maps of B, C, and D clusters in anaerobic A559/V610 variants

The F_o–F_c difference electron-density maps of B, C, and D clusters in A559/V610 variants under anaerobic conditions are contoured at 3 σ. Fe, S, and Ni atoms are colored in orange, yellow and green, respectively.

	D cluster (9.0 σ)	B cluster (9.0 σ)	C cluster (4.5 σ)
ChCODH2 WT PDB : 1SU7	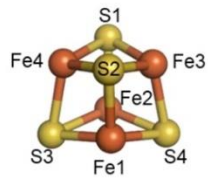	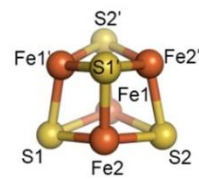	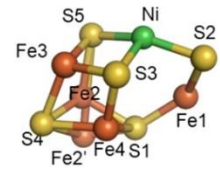
Anaerobic WH (A559W/V610H)	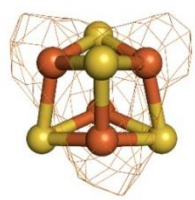	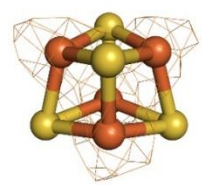	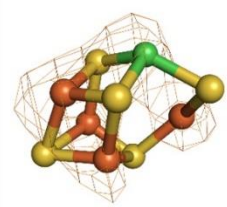
Anaerobic WW (A559W/V610W)	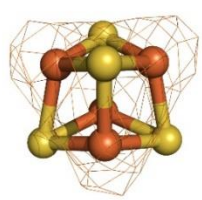	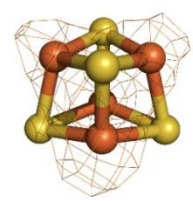	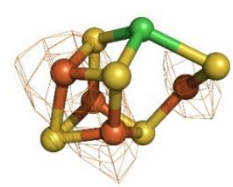
Anaerobic HH (A559H/V610H)	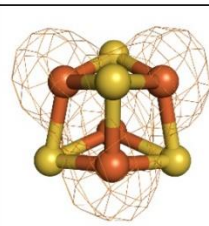	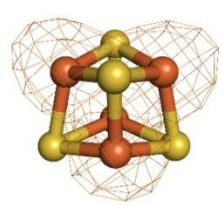	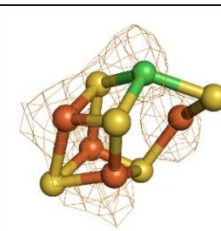

Figure 3.3 Fe anomalous difference map in anaerobic A559/V610 double variants

Fe anomalous difference Fourier maps illustrating the positions of Fe atoms in B, C, and D clusters are shown in orange mesh. The F_o-F_c difference electron densities are contoured at 9.0, 9.0, and 4.5 σ in each cluster.

3.3. Tunnel analysis in bottleneck points

To investigate the impact of mutations at A559 and V610 with histidine and tryptophan on the gas tunnel associated with the active site C-cluster, I conducted tunnel analysis using the CAVER program (Chovancova et al., 2012), comparing to the *Ch*CODH- II WT (PDB ID: 1SU7). Consistent with previous studies, two major types of gas tunnels were identified: the main CO (CO_2) tunnel and the Non-selective gas tunnel, which allows the passing of any gas, e.g., CO, O_2, or H_2O. Among these two tunnels, the double mutant at the A559 and V610 sites specifically influenced the non-selective gas tunnel. Compared to *Ch*CODH-II WT, all three variants exhibited a narrowing of the tunnels. The V610H mutant appears to have lost the tunnel; however, the V610W mutant still retains the narrower tunnel. Notably, the A559W/V610H variant exhibited the most significant narrowing of the tunnel entrance, with A559W causing a reduction from 1.66 Å to 0.84 Å and V610H reduced 1.31 Å to 0.83 Å when compared to *Ch*CODH- II WT (Figure 3.4A). As a result, the narrower non-selective gas tunnel connected to the C-cluster significantly reduces the possibility of oxygen exposure induced by the surface bottleneck key site V610H and the internal bottleneck key site A559W at the same time (Figure 3.4B).

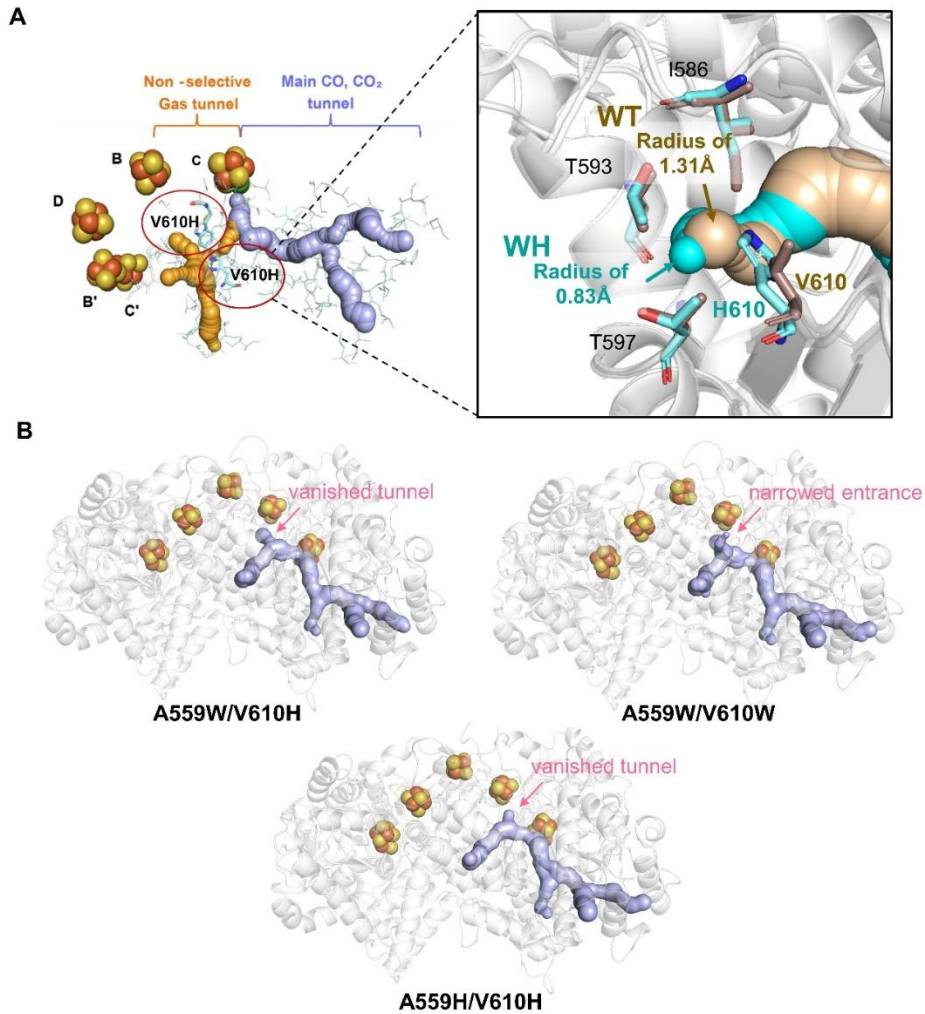

Figure 3.4 Gas tunnels and tunnel obstruction of *Ch*CODH-II A559/V610 double variants

A. Gas tunnels (non-selective gas tunnel and main CO/CO_2 tunnel) in *Ch*CODH-II A559/V610 variants. Tunnel obstruction in WH (A559W/V610H) variant compared to WT. **B.** Observation of tunnel changes in *Ch*CODH-II A559/V610 variants.

3.4. Comparing the time scale of O_2 exposure between *Ch*CODH-II WT and the WH (A559W/V610H) variant

To cover a more precise understanding of oxygen resistance, I examined crystallization involving prolonged exposure to oxygen. Upon the structural insights under anaerobic conditions, the WH (A559W/V610H) variant has a narrower tunnel and higher stability then the *Ch*CODH-II WT (PDB ID:1SU7). Each anaerobically purified protein was exposed to oxygen for 2 hours outside of the chamber and than crystallization was performed under the anaerobic conditions. Firstly, the local environments of the A559 and V610 residues in both the WT and WH mutant was examined. The 2 hours oxygen exposed WH variant were consistent with anaerobic results, showing that these residues were well-preserved and their interactions remained unchanged. Secondly, the 2 hours oxygen exposed *Ch*CODH-II WT of the D and C clusters exhibited almost decay in both the omit map (*Fo-Fc*) (Figure 3.5) and the Fe anomalous map (Figure 3.6) compared to the WH variant, which was still intact. The WT failed to make a proper map of both omit and Fe anomalous map. Additionally, Unlike the WH variant, in the case of the WT, the B-factors of the proteins and clusters indicate numbers 95 and 148, suggesting that the overall structure might be degraded. This result allows us to understand the reason behind the loss of activity observed when exposing the sample to oxygen for 2 hours. Thirdly, tunnel analysis was conducted using the CAVER program. The WH variant, oxygen exposed for 2 hours,

exhibited the same pattern as the anaerobic WH variant, with A559W and V610H causing a reduction from 1.66 Å to 0.78 Å and 1.31 Å to 0.86 Å when compared to *Ch*CODH- II WT (Figure3.7A). Given these evidence, I concluded that the WH (A559W/V610H) variant has a much higher oxygen resistance than the *Ch*CODH-II WT.

	D cluster (3.0 σ)	B cluster (3.0 σ)	C cluster (2.5 σ)
ChCODH2 WT PDB : 1SU7	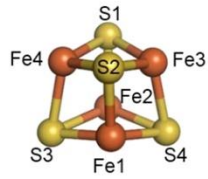	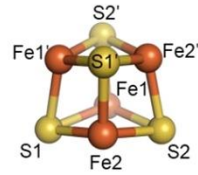	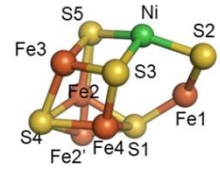
2hour O_2 exposure WH (A559W/V610H)	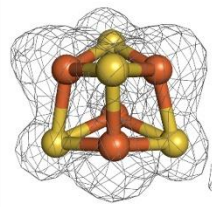	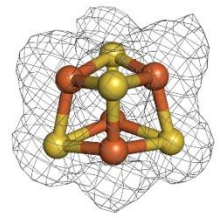	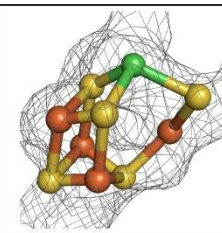
2hour O_2 exposure WT	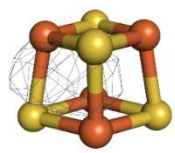	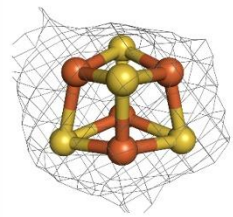	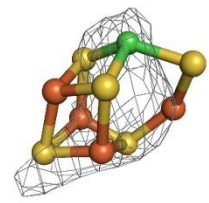

Figure 3.5 *Fo–Fc* difference electron density maps of B, C, and D clusters in oxygen exposure A559 / V610 variants

Fo–Fc difference electron-density maps of B, C, and D clusters in A559/V610 double variants under 2 hours oxygen exposure condition are contoured at 3, 3 and 2.5 σ. Fe, S, and Ni atoms are colored in orange, yellow and green, respectively.

	D cluster (9.0 σ)	B cluster (9.0 σ)	C cluster (5.5 σ)
ChCODH2 WT PDB : 1SU7	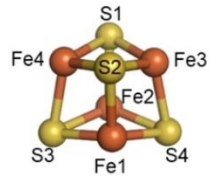	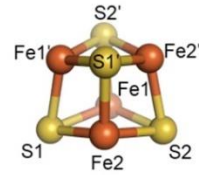	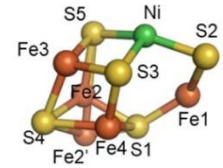
2hour O_2 exposure WH (A559W/V610H)	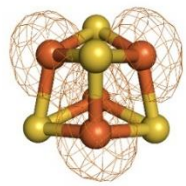	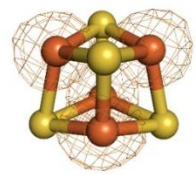	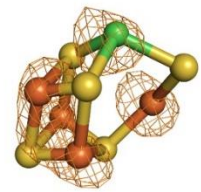
2hour O_2 exposure WT	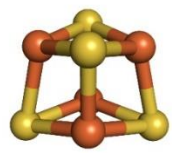	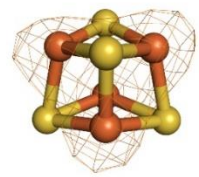	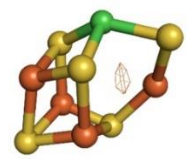

Figure 3.6 Fe anomalous difference map in oxygen exposure A559 / V610 variants

Fe anomalous difference Fourier maps illustrating the positions of Fe atoms in B, C, and D clusters are shown in orange mesh. The F_o-F_c difference electron densities are contoured at 9.0, 9.0, and 5.5 σ in each cluster.

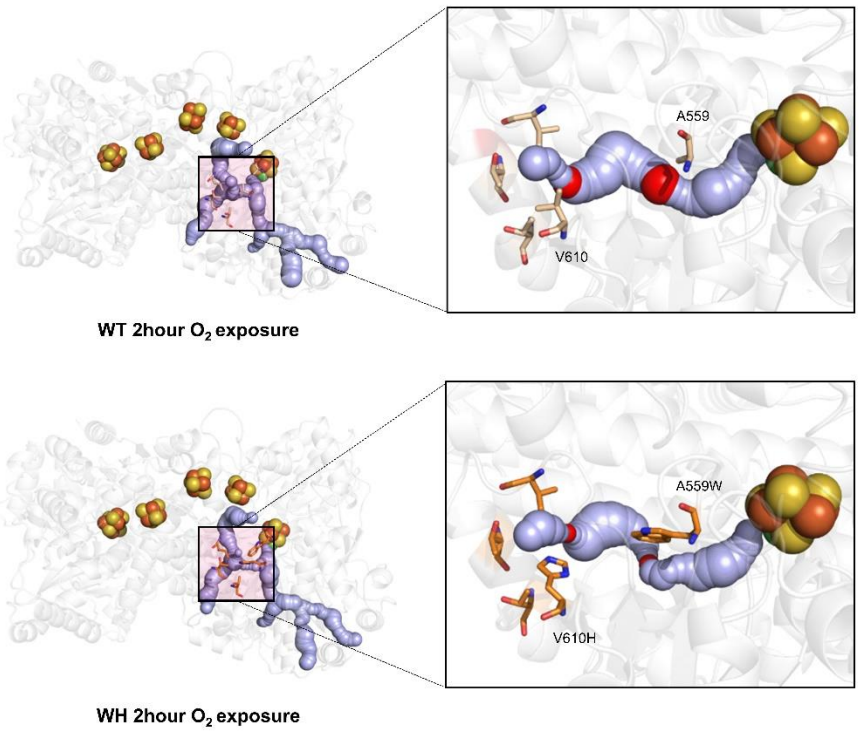

Figure 3.7 Gas tunnels and tunnel obstruction of 2 hour O_2 exposed *Ch*CODH-II A559/V610 double variants

Gas tunnels (non-selective gas tunnel and main CO/CO_2 tunnel) in *Ch*CODH-II WT and A559/V610 variant. The non-selective tunnel 2 bottleneck of A559 and V610 is in red.

4. Conclusion

CO is a major air pollutant commonly found in industrial emissions. Converting CO into other forms has been challenging due to its expensive cost, but the utilization of CODHs (Carbon monoxide dehydrogenase) can easily convert CO into CO_2, making it suitable for renewable energy or various applications. However, CODH has a significant limitation in losing its CO oxidation activity under aerobic conditions. To overcome this limitation, a previous study focused on enhancing the oxygen tolerance of the *Ch*CODH-II, which has the highest CO conversion activity, by mutating the A559 site to bulky aromatic residues such as tryptophan, histidine, or serine, similar to *Dv*CODH or *Ch*CODH-IV. However, these modifications only maintain the activity under low O_2 conditions, typically in the 0.1-0.5% range. Here, we suggested that the mutation of A559 and V610 sites would sustain CO conversion activity even under higher oxygen condition (20% O_2).

In summary, the V610 site is located at the surface bottleneck in the non-selective tunnel of the C-cluster. As I mutated A559 and V610 residues to large aromatic residues, tryptophan, and histidine, I confirmed that oxygen resistance had been enhanced from the crystal structure determination and tunnel analysis. Through activity tests, the *Ch*CODH-II variants exhibited more significant activity than the *Ch*CODH-II WT and A559 single variants under 20% oxygen. Based on the structure results, I concluded that mutating

small residues such as A559 or V610 to larger aromatic ring residues like tryptophan or histidine makes the tunnel entrance narrower (reduction from 1.66 Å to 0.84 Å and 1.31 Å to 0.83 Å), selectively blocking O_2. This effect allows protection of the C-cluster active site from oxygen. The A559W/V610H residue aligned well with the map, and no other residues were affected. Unfortunately, the WW variant of V610W residue was disordered, affecting I580, L583, and L612 residues. For these reasons, I concluded that the V610H is the most proper mutation for the O_2 tolerant model. An oxygen exposure experiment was conducted to determine more precise reasons for oxygen resistance. The response of the *Ch*CODH-II WH (A559W/V610) variant and the WT to 2 hours oxygen exposure was compared using the omit map (F_o-F_c) and Fe anomalous map. I discovered that the D and C clusters in the WT were degraded, while the clusters of the WH (A559W/V610) variant remained intact. Also, the 2-hour oxygen-exposed WH variant's tunnel was same as the anaerobically WH variant. The comparison clearly demonstrated that the WH variant has significantly higher oxygen tolerance than *Ch*CODH-II WT. These results suggest the possibility of developing Ni-Fe CODHs with complete oxygen resistance for potential industrial applications, such as carbon reduction, gas cleaning, and renewable energy technologies.

Appendix

I. O_2 Catalytic properties of *Ch*CODH-II double variants[3]

Mutations were introduced to bulk, charge, polarity, and hydrophobicity effects to determine the potential effects of key position residues in the Non-selective tunnel 1-3 of *Ch*CODH-II. During this process, we performed single mutations on tunnels 1-3 and simultaneously mutations of the key residues in tunnels 1-3 after mutating A559 to tryptophan, serine, or histidine. Mutation of the CO Non-selective tunnel 1 and 3 of key residues resulted in an approximately 20-fold decrease in expression levels compared to *Ch*CODH-II WT. We also observed a few notable results: not only did the E43H/K450H mutant show no activity, but also L587H seemed to enhance oxygen resistance. It exhibited a similar pattern with tunnel 1 and 3 mutations with a significantly low expression level. Given that mutations in Non-selective CO tunnels 1 and 3 could enhance oxygen resistance but adversely affect expression levels due to impact on protein folding or structural stability, we shifted focus on the key residues in tunnel 2 (Table I). In tunnel 2, mutations of V610 to tryptophan and histidine showed the highest specific activity in enhancing oxygen resistance (Figure I). Among them, the HH (A559H/V610H) double mutant had slightly higher oxygen tolerance, but

[3] Activity tests were done by Suk Min Kim, Ph. D. and Jinhee Lee in Ulsan National Institute of Science and Technology (UNIST).

protein stability and expression level was lower than WH (A559W/V610H) and WW (A559W/V610W) double mutants. Structural analysis was conducted to analyze which variants possess the highest oxygen resistance.

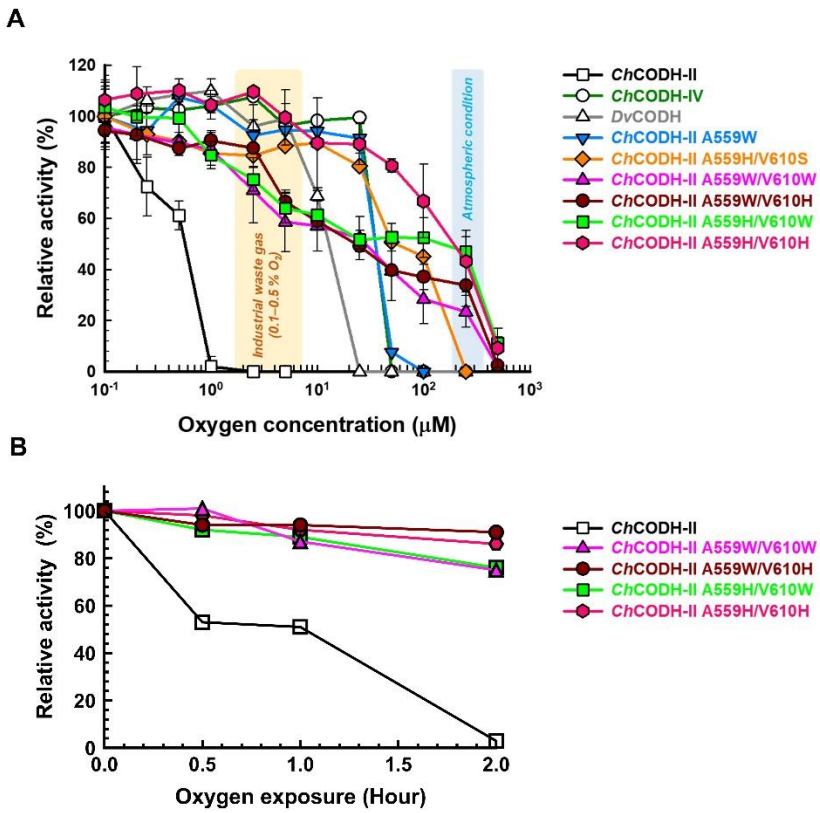

Figure I. Activity tests for O_2 tolerance in *Ch*CODH-II A559 and V610 variants.

A. Reduced O_2 tolerance in Ni-Fe CODHs and variants. These variants were expressed in *E. coli* and purified with Ni-NTA affinity. Variants were exposed to 250 μM O_2, which is almost atmospheric condition, and then their CO oxidation activities were screened. Before assay, the CODHs (2-4 μg) were incubated in 50mM HEPES (final volume of 200 μl) for 2min with O_2 addition, and then the reaction mixture was diluted 200-400 times to give a final O_2 concentration below 0.6μM. Investigating the impact of varying O_2 concentrations on Ni-Fe CODHs (open symbols) and engineered *Ch*CODH-

II variants (closed symbols): *Ch*CODH-II (squares), *Ch*CODH-IV (circles), DvCODH (triangles), *Ch*CODH-II A559W (reverse triangles), *Ch*CODH-II HS (diamonds), *Ch*CODH-II WW (triangles), *Ch*CODH-II WH (circles), *Ch*CODH-II HW (squares), *Ch*CODH-II HH (hexagons). The data represent the mean ± S.D., as determined from $n = 3$ independent experiments. **B.** Reduced O_2 tolerance in the 2 h O_2 exposed *Ch*CODH-II WT and variants. *Ch*CODH-II WT (open square symbols) and engineered *Ch*CODH-II variants (closed symbols): *Ch*CODH-II WW (triangles), *Ch*CODH-II WH (circles), *Ch*CODH-II HW (squares), *Ch*CODH-II HH (hexagons). The data represent the mean ± S.D., as determined from $n = 3$ independent experiments

Table I. Summary of O_2 tolerance in tested variants

Tunnel	Name	Specific activity (U/mg)
	*Ch*CODH-II WT	1,300 ± 108.5
Non-selective tunnel#1	E43H	0
	K450H	0
	L583H	180 ± 0.8
Non-selective tunnel#2	A559W / V610H	1,179.5 ± 294.6
	A559W / V610W	795.8 ± 210.3
	A559H / V610H	483.6 ± 129.8
	A559H / V610W	210.2 ± 25.9
Non-selective tunnel#3	Q206H	0
	S599H	0
	I603H	0

* Enzymatic activities used to assay O_2 sensitivity are calculated as the mean of three independent measurements.

Reference

Choi, E. S., Min, K., Kim, G. J., Kwon, I. and Kim, Y. H. (2017). Expression and characterization of *Pantoea* CO dehydrogenase to utilize CO-containing industrial waste gas for expanding the versatility of CO dehydrogenase. *Sci. Rep*. ***7***, 44323.

Chovancova, E., Pavelka, A., Benes, P., Strnad, O., Brezovsky, J., Kozlikova, B., Gora, A., Sustr, V., Klvana, M., Medek, P., Biedermannova, L., Sochor, J and Damborsky, J. (2012). CAVER 3.0: A tool for the analysis of transport pathways in dynamic protein structures. *PLOS Comput. Biol* ***8***, e1002708.

Darden, T., York, D., and Pedersen, L. (1993). Particle mesh Ewald: An N·log(N) method for Ewald sums in large systems. *J. Chem. Phys*. ***98***, 10089-10092.

Dobbek, H., Svetlitchnyi, V., Gremer, L., Huber, R., and Meyer, O. (2001). Crystal structure of a carbon monoxide dehydrogeanse reveals a [Ni−4Fe−5S] cluster. *Sience* ***293***, 1281-1285.

Dobbek, H., Svetlitchnyi, V., Liss, J., and Meyer, O. (2004). Carbon monoxide induced decomposition of the active site [Ni−4Fe−5S] cluster of CO dehydrogenase. *J. Am. Chem. Soc*. ***126***, 5382-5387.

Domnik, L., Merrouch, M., Goetzl, S., Jeoung, J.H., Léger, C., Dementin, S., Fourmond, V., and Dobbek, H. (2017). CODH-IV: A high-efficiency CO-scavenging CO dehydrogenase with resistance to O_2. *Angew. Chem. Int. Ed. Engl.* ***56***, 15466-15469.

Drake, H.L. (1982). Occurrence of nickel in carbon monoxide dehydrogenase from *Clostridium pasteurianum* and *Clostridium thermoaceticum*. *J. Bacteriol.* ***149***, 561-566.

Drennan, L., Heo, J., and Sintchak, M. (2001). Life on carbon monoxide: X-ray structure of Rhodospirillum rubrum Ni-Fe-S carbon monoxide dehydrogenase. *Proc. Natl. Acad. Sci*. ***98***, 11973-11978.

Emsley, P., and Cowtan, K. (2004). Coot: model-building tools for molecular graphics. *Acta Crystallogr. D Biol. Crystallogr.* ***60***, 2126–2132.

Hwang, H.W., Yoon, J., Min, K., Kim, M.-S., Kim, S.J., Cho, D.H., Susila, H., Na, J.-G., Oh, M.K., and Kim, Y.H. (2020). Two-stage bioconversion of carbon monoxide to biopolymers via formate as an intermediate. *Chem. Eng. Sci*. ***389***, 124394.

Jeoung, J.H., Martins, B.M., and Dobbek, H. (2019). X-ray crystallography of Carbon monoxide dehydrogenases. *Methods Mol. Biol.* ***1876***, 167-178.

Kim, S. M., Lee, J. H., Kang, S.H., Heo, Y. Y., Yoon, H.J., Hahn, J.S., Lee, H.H., and Kim, Y. H. (2022). O_2 tolerant CO dehydrogeanse via tunnel

redesign for the removal of CO from industrial flue gas. *Nat. Catal*. **5**, 807-817

Kim, T.W., Bae, S.S., Lee, J.W., Lee, S.M., Lee, J.H., Lee, H.S., and Kang, S.G. (2016). A biological process effective for the conversion of CO-containing industrial waste gas to acetate. *Bioresour Technol*. ***211***, 792-796.

Liebgott, P.-P., Leroux, F., Burlat, B., Dementin, S., Baffert, C., Lautier, T., Fourmond, V., Ceccaldi, P., Cavazza, C., Meynial-Salles, I., Soucaille, P., Guigliarelli, B., Bertrand, P., Rousset, M and Leger, C. (2010). Relating diffusion along the substrate tunnel and oxygen sensitivity in hydrogenase. *Nat. Chem. Biol* ***6***, 63-70.

Liebschner, D., Afonine, P.V., Baker, M.L., Bunkoczi, G., Chen, V.B., Croll, T.I., Hintze, B., Hung, L.W., Jain, S., McCoy, A.J., Moriarty, N., Oeffner, R.,, Poon, B., Prisant, M., Read, R., Richardson, J., et al. (2019). Macromolecular structure determination using X-rays, neutrons and electrons: recent developments in Phenix. *Acta Crystallogr. D Biol. Crystallogr.* ***75***, 861-877.

Merrouch, M., Hadj-Saïd, J., Domnik, L., Dobbek, H., Léger, C., Dementin, S., and Fourmond, V. (2015). O_2 inhibition of Ni-containing CO dehydrogenase is partly reversible. *Chem. Eur. J.* ***21***, 18934-18938.

Otwinowski, Z., and Minor, W. (1997). Processing of X-ray diffraction data collected in oscillation mode. *Methods Enzymol* ***276***, 307-326.

Ragsdale, S. W. (2004). Life with carbon monoxide. *Crit. Rev. Biochem. Mol. Biol.* ***39***, 165–195.

Rovaletti, A., Bruschi, M., Moro, G., Cosentino, U., and Greco, C. (2019). The challenging in silico description of carbon monoxide dxidation as catalyzed by molybdenum-copper CO dehydrogenase. *Front. Chem*. ***6***, 630

Svetlitchnyi, V., Peschel, C., Acker, G., and Meyer, O. (2001). Two membrane-associated Ni-Fe-S carbon monoxide dehydrogenases from the anaerobic carbon monoxide utilizing eubacterium *Carboxydother mus hydrogenoformans*. *J. Bacteriol.* ***183***, 5134-5144.

Winn, M.D., Ballard, C.C., Cowtan, K.D., Dodson, E.J., Emsley, P., Evans, P.R., Keegan, R.M., Krissinel, E.B., Leslie, A.G., McCoy, A., McNicholas, S., Murshudov, G., Pannu, N., Potterton, E., Powell, H., Read, R., Vagin, A., and Wilson, K. (2011). Overview of the CCP4 suite and current developments. *Acta Crystallogr. D Biol. Crystallogr.* ***67***, 235-242.

Wu, M., Ren, Q., Durkin, A.S., Daugherty, S.C., Brinkac, L.M., Dodson, R.J., Madupu, R., Sullivan, S.A., Kolonay, J.F., Nelson, W., Tallon, L., Jones, K., Ulrich, L., Gonzalez, J., Zhulin, I., Robb, F., and Eisen, J. (2005).

Life in hot carbon monoxide: the complete genome sequence of *Carboxydothermus hydrogenoformans* Z-2901. *PLoS Genet*. ***1***, 563–574.

Zhang, B., Hemann, C.F., and Hille, R. (2010). Kinetic and spectroscopic Studies of the Molybdenum-Copper CO dehydrogenase from *Oligotropha carboxidovorans*. *J. Biol. Chem.* ***285***, 12571-1257

국문 초록

산소저항성을 높인

carbon monoxide dehydrogenase

(CODH)구조 규명 연구

공소연

자연과학대학 화학부

서울대학교 대학원

*Carboxydothermus hydrogenoformans*로부터 분리된 *Ch*CODH-II는 일산화탄소를 이산화탄소로 산화시킬 수 있는 혐기성효소이다. 이 효소는 다른 CODH들과 비교하여 일산화탄소의 산화 속도가 빠른 편이지만 산소에 민감하여 실제적인 응용에 어려움이 있다. 이러한 문제를 극복하기 위해, 선행연구에서 C-cluster와 연결된 가스 터널의 내부 병목 위치인 A559 잔기에 큰 방향족 링을 가지는 히스티딘, 트립토판 및 세린으로 돌연변이를 도입하는 연구를 진행하였다. 그러나 이러한 돌연변이 형태는 낮은 산소 농도(0.1-0.5% 산소)에서만 활성을 유지할 수 있다는 한계점이 있다. 따라서 본 연구에서는 대기와 같은 산소 조건(20% 산소)에서도 활성을 유지할 수 있는 *Ch*CODH-II를 개발하기 위해 C-cluster와 연결되면서 비선택적 터널의 표면 근처에 위치한 V610에 추

가적으로 히스티딘과 트립토판으로 돌연변이를 도입하여 산소 저항성을 향상시키는 연구를 수행하였다. 이를 위해 혐기성 조건에서 결정화된 구조를 분석하여 돌연변이의 산소 저항성 증가 원인을 밝혔다. 또한, 터널 분석을 통해 *Ch*CODH-II WT과 대비하여 돌연변이를 도입한 잔기들의 주변 터널 입구가 좁아지는 것을 확인하였다. 더 나아가, 산소를 노출시켰을 때 돌연변이도입체가 *Ch*CODH-II WT과 대비하여 구조적으로 잘 유지되고 있는지 확인하기위해 2시간 동안 산소에 노출시켜 결정화를 진행하였다. 결과적으로 omit (F_o-F_c)과 Fe anomalous map 을 통해 *Ch*CODH-II WT의 D 와 C 클러스터는 무너졌지만 WH(A559W/V610)는 혐기성 WH와 동일하게 유지되고 있음을 확인하였으며, 터널 분석에서도 WH의 터널이 좁아진 것을 확인하였다. 본 연구를 통해 A559와 V610잔기에 큰 방향족 링을 가지는 히스티딘과 트립토판으로 돌연변이를 도입하면 비선택적 가스 터널이 좁아져서 산소가 통과하지 못하게 되어 산소저항성이 크게 증가함을 밝혔다.

주요어 : Carbon monoxide dehydrogenase, *Ch*CODH-II, 결정화, 산소 저항성, CO 산화

학번 : 2021-27351